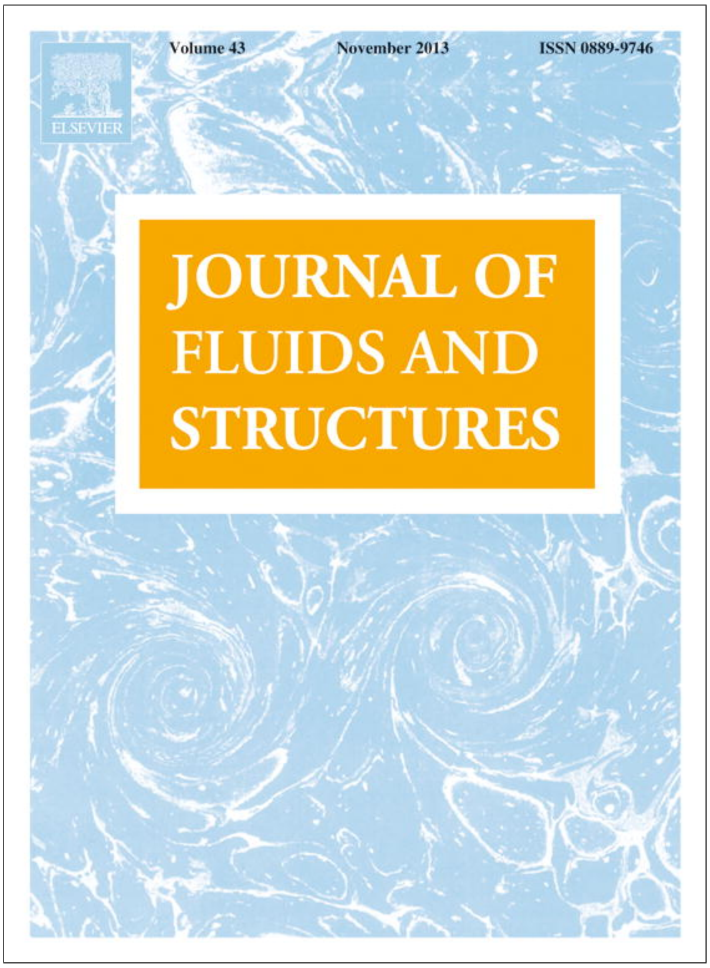
Volume 43
November 2013
ISSN 0889-9746
ELSEVIER
JOURNAL OF FLUIDS AND STRUCTURES

Journal of Fluids and Structures 43 (2013) 325–346

Contents lists available at ScienceDirect

Journal of Fluids and Structures

journal homepage: www.elsevier.com/locate/jfs

Immersed boundary modeling for interaction of oscillatory flow with cylinder array under effects of flow direction and cylinder arrangement

Ming-Jyh Chern [a,*], Wei-Cheng Shiu [a], Tzyy-Leng Horng [b]

[a] Department of Mechanical Engineering, National Taiwan University of Science and Technology, 43 Section 4 Keelung Road, Taipei 10607, Taiwan
[b] Department of Applied Mathematics, Feng Chia University, Taichung 40724, Taiwan

ARTICLE INFO

Article history:
Received 21 August 2012
Accepted 23 September 2013
Available online 17 October 2013

Keywords:
Direct-forcing immersed boundary method
Circular cylinders array
Oscillatory flow
Fluid–structure interaction

ABSTRACT

An array of cylindrical structures are often used as a frame of an offshore platform. The prediction of hydrodynamic loadings on those cylindrical structures due to oscillatory flows is one of the most important issues in the design of those offshore structures. The aim of this study is to apply a direct-forcing immersed boundary method to simulating the oscillatory flow past a circular cylinder array in a square arrangement. The finite volume method was used to solve the Navier–Stokes equations. In this study, the effects of Keulegan–Carpenter (KC) number, oblique flow and the gap among four cylinders were investigated. Numerical results were visualized using vorticity contours so evolutions of oscillatory flow with the cylinder array were presented. Hydrodynamic loadings including in-line and transverse force coefficients were determined and illustrated in the time and spectral domains. Essentially, the proposed direct-forcing immersed boundary approach can be useful for scientists and engineers who would like to understand the interaction of the oscillatory flow with an array of cylinders and to estimate hydrodynamic loadings on the array of cylinders.

1. Introduction

The interaction between an oscillatory flow and structures often occurs in nature and numerous engineering applications. For example, to obtain oil in an offshore region, a tension-leg platform is used and encounters oscillatory flows due to a wave train or tide. Another example is a wave energy power station which may consists of a cylinder array for its frame (see Langlee, 2006). Those structures with a circular cylinder array in an offshore region receive hydrodynamic loadings from waves. While predicting the hydrodynamic loadings on the circular cylinders, it is important to explore the temporal variation of hydrodynamic loadings on those cylinders. For example, the so-called "ringing" effect refers to a fast and high frequent hydrodynamic damage on an offshore platform (see Spidsoe and Karunakaran, 1996). Due to this reason, the oscillatory flow around a circular cylinder array has been studied by Anagnostopoulos and Dikarou (2011). The aim of this study is to establish a numerical model to predict the hydrodynamic loading on circular cylinders using an immersed boundary method.

* Corresponding author. Tel.: +886 2 27376496; fax: +886 2 27376460.
E-mail address: mjchern@mail.ntust.edu.tw (M.-J. Chern).

0889-9746/$ - see front matter © 2013 Elsevier Ltd. All rights reserved.
http://dx.doi.org/10.1016/j.jfluidstructs.2013.09.022

Nomenclature

C_f	in-line force coefficient, $-2F_{in}$
C_l	transverse force coefficient, $-2F_t$
$\overline{C}_f$	root mean square of in-line force coefficient
$\overline{C}_l$	root mean square of transverse force coefficient
D	dimensionless diameter of cylinder
F_{in}	dimensionless force in the flow direction
F_t	dimensionless force in the transverse direction
f	dimensionless frequency of C_l
f_o	dimensionless frequency of oscillatory flow
$\mathbf{F}$	total dimensionless virtual force
$\mathbf{f}$	dimensionless virtual force per unit mass
KC	Keulegan–Carpenter number, U_mT/D
P	dimensionless distance between of two neighboring cylinders
p	dimensionless pressure
R	dimensionless radius of cylinder
Re	Reynolds number, U_mD/ν
T	dimensionless period of oscillating flow
t	dimensionless time
U_m	amplitude of oscillating flow
$\mathbf{u}(u,v)$	dimensionless velocity
x, y	dimensionless Cartesian coordinates

Greek symbols

β	viscous parameter, Re/KC
η	the volume of solid function
ν	kinematic viscosity of fluid, $m^2\,s^{-1}$

Subscripts

s	solid

Superscripts

m	time level
$*$	intermediate time level

The oscillatory flow past cylinders has attracted the interest of researchers in the past few decades. Sarpkaya (1986) performed an experiment to measure the in-line force coefficients for a circular cylinder in planar oscillatory flows with small amplitudes. He provided theoretical and experimental results of inertia coefficient and flow visualization. Subsequently, Obasaju et al. (1988) measured the total forces and spanwise correlation of vortex shedding was presented for a circular cylinder in the planar oscillatory flow. The flow variations were classified as the asymmetric, the transverse, the diagonal, the third vortex, and the quasi-steady regimes at Keulegan–Carpenter numbers from 4 to 55 and the viscous parameter β from 100 to 1665. Sumer and Fredsoe (1997) reviewed previous studies about the oscillatory flow around a circular cylinder. They described the flow pattern and the resulting load when the waves or currents interact with a cylinder. Kuhtz et al. (1997) measured forces on immersed bodies at low Reynolds numbers in an oscillatory flow. With the increase in efficiency of digital computers, a number of researchers studied the interaction between the oscillatory flow and cylinders by numerical simulations. Iliadis and Anagnostopoulos (1998) used the finite element method to investigate the oscillatory flow around a circular cylinder at low KC numbers and varying β. The in-line and the transverse forces on the circular cylinder were determined and reported. Zheng and Dalton (1999) used the finite difference method to study oscillatory flow past a square cylinder at KC numbers up to 5. They presented flow patterns around a square cylinder and predicted force on the square cylinder. The influence of blockage ratio was investigated by Anagnostopoulos and Minear (2004). They described the effect of the width of the computational domain on an oscillatory flow past a circular cylinder. By altering the blockage ratio, they investigated the influences of the hydrodynamic force and vortices on cylinders. The results showed that the blockage effect cannot be neglected for the blockage ratio higher than 20%. An et al. (2006) study the oscillatory flow past two cylinders in a tandem arrangement. They investigated the effect of the gap between two cylinders and KC numbers. Recently, An et al. (2011) simulated the three dimensional oscillatory flow around a circular cylinder at low KC numbers. They found that the spacing between Honji vortices is strongly correlated with KC number. Zhao et al. (2011) simulated a three dimensional oscillatory flow around a circular cylinder at right and oblique attacks. They described streamlines around the cylinder at successive time steps and compared the hydrodynamic forces with the right attack case. Suthon and Dalton (2011) established a 3-D finite-difference spectral scheme to explore the 3-D flow around an oscillating circular cylinder at low KC number. They reported the mushroom structures in the near wake which are called the Honji instability.

The flow past two or more cylinders has been reported in a number of published manuscripts. Williamsion (1985) employed the flow visualization technique to study an oscillatory flow past a circular cylinder and a pair of circular cylinders at different KC numbers. A pair of cylinders in side-by-side, oblique and tandem arrangements were considered in experiments. He studied the effect of gap between two cylinders on flow variation and hydrodynamic forces. Chern et al. (2010) studied the interaction of oscillatory flows with a pair of side-by-side square cylinders. They investigated the influence with various KC numbers, Reynolds numbers, and cylinder gap. Anagnostopoulos and Dikarou (2011) carried out the viscous oscillatory flow past four cylinders at β=50 and KC range from 0.2 to 10. The hydrodynamic forces on those cylinders, flow field and the effect of pitch ratio were reported. Lam and Zou (2010) presented the three dimension numerical simulations of cross flow around four cylinders. They investigated the effect of spacing ratio and aspect ratio and illustrated the difference between 2-D and 3-D simulations.

The capability to handle complex geometries and computational time has been the main issues in computational fluid dynamics. An immersed boundary method has been proven to be able to deal with a complex geometry and a moving body. The immersed boundary method has been getting popular in recent years since it was introduced by Peskin (1973). A virtual force due to the existence of a solid object is used as a body force in the momentum equation while Peskin's immersed boundary method is adopted. A Dirac delta function is employed to distribute the virtual force from the solid object to the fluid flow. The immersed boundary method which added a virtual force in the momentum equations to simulate the effect of solid. One of the immersed boundary methods is the so-called direct-forcing method proposed by Yusof (1996). The direct-forcing method determines a forcing term by calculating the difference between the interpolated velocities on the boundary points and the desired solid boundary velocities. This idea of the direct-forcing method has been adopted and obtained successful applications. Fadlun et al. (2000) developed combined immersed boundary finite difference methods for three dimensional complex flow simulations. Su et al. (2007) used the immersed boundary technique for the simulation of flow interacting with solid boundary. Noor et al. (2009) study the fluid–solid interaction problems using the current proposed direct-forcing immersed boundary method.

The aim of this study is to apply a direct-forcing immersed boundary method to simulating the oscillatory flow past four circular cylinders array in a square arrangement. To investigate the influences of KC number, the flow direction, and the gap ratio, hydrodynamic forces, flow patterns and phase diagrams were discussed in the study.

2. Mathematical formulae and numerical model

In this study, the direct-forcing immersed boundary method is used to simulate a solid object in fluid flow. In order to solve the interaction between fluids and solids, a virtual force is added to Navier–Stokes equations for incompressible fluid flow. Details of governing equations for fluids and the direct-forcing immersed boundary methods are explained in the following sections.

2.1. Governing equations

An incompressible viscous fluid is considered in the present study. Following the rules of conservation of mass and momentum, we adopt dimensionless form shown as

$$\nabla \cdot \mathbf{u} = 0 \tag{1}$$

and

$$\frac{\partial \mathbf{u}}{\partial t} + \nabla \cdot (\mathbf{u}\mathbf{u}) = -\nabla p + \frac{1}{\mathrm{Re}}\nabla^2 \mathbf{u} + \mathbf{f}, \tag{2}$$

where $\mathbf{u}$ and p are dimensionless velocity and pressure, respectively. Re is the Reynolds number and denoted by $U_m D/\nu$, where U_m is the amplitude of the oscillatory flow, D is the cylinder diameter and ν is the kinematic viscosity of the fluid. It should be noted that there is a virtual force term denoted as $\mathbf{f}$ in Eq. (2). This term is added in order to accommodate interaction between solids and fluids. It is determined from

$$\mathbf{f} = \eta \frac{\mathbf{u_s} - \mathbf{u_f}}{\Delta t}, \tag{3}$$

where η is defined as the volume fraction of a solid at a computational cell. If a cell is full of solids, then η will be 1. On the other hand, η is equal to zero for a cell full of fluids. In this study, η is located at the center of a computational cell. For example, consider a circular cylinder in the flow domain. If the distance between the center of the cylinder and the center of a cell is less than the radius of the cylinder, then η will be 1. On the other hand, η is zero when the distance is greater than the radius. The prescribed velocity of the solid is $\mathbf{u_s}$. In this study, cylinders are fixed so $\mathbf{u_s}$ is zero for all cylinders.

2.2. Oscillatory flow boundary condition

In order to simulate the flow due to a progressive wave train, oscillatory flows are considered in this study. Transient velocity boundary conditions are imposed at four boundaries of the computational domain to simulate oscillatory flows as shown in Fig. 1. Consider an oscillatory flow of dimensionless period T. The dimensionless horizontal velocity component of the oscillatory flow varies according to the condition

$$u = \sin\left(\frac{2\pi t}{T}\right) \quad \text{and} \quad v = 0, \tag{4}$$

while boundary conditions of the oblique flow are given as

$$u = \sin\left(\frac{2\pi t}{T}\right)\cos\left(\frac{\pi}{4}\right) \quad \text{and} \quad v = \sin\left(\frac{2\pi t}{T}\right)\sin\left(\frac{\pi}{4}\right). \tag{5}$$

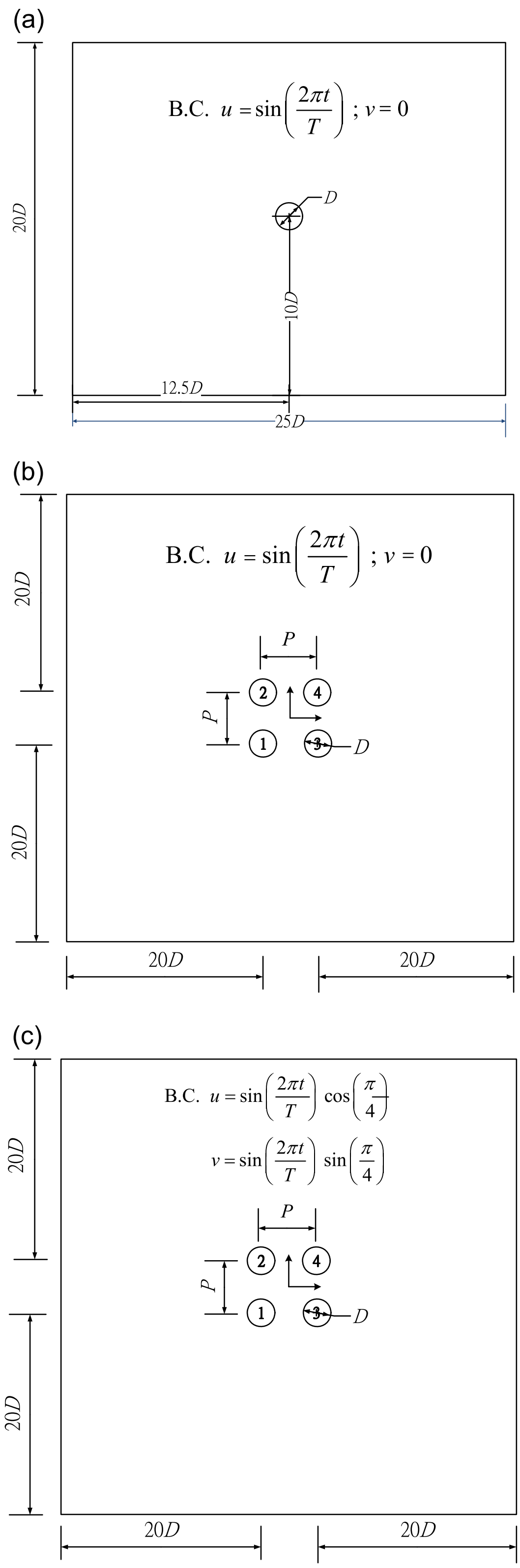

Fig. 1. Schematic of interaction of (a) a horizontal oscillatory flow with a single circular cylinder, (b) a horizontal oscillatory flow with four circular cylinders, (c) an oblique oscillatory flow with four circular cylinders.

2.3. *Calculation of hydrodynamic force on cylinder*

In this study, the integral of the virtual force will be approximation of the dimensionless resultant force exerted on a single circular cylinder, i.e.,

$$\mathbf{F} = \iiint_{\Omega} \mathbf{f} \, dV. \tag{6}$$

Subsequently, the in-line and lift force coefficients, C_f and C_l, can be determined from

$$C_f = -2 \cdot F_{in} \tag{7}$$

and

$$C_l = -2 \cdot F_t, \tag{8}$$

respectively. The r.m.s. values of in-line force and transverse force in dimensionless form are defined as

$$\overline{C}_f = \left(\frac{1}{T}\int_0^T C_f^2\, \mathrm{d}t\right)^{1/2} \tag{9}$$

and

$$\overline{C}_l = \left(\frac{1}{T}\int_0^T C_l^2\, \mathrm{d}t\right)^{1/2}, \tag{10}$$

as mentioned in Anagnostopoulos and Dikarou (2011), respectively.

2.4. Numerical procedures

The momentum equation, Eq. (2), is solved in three steps. First, the velocity is stepped from the nth time level to the first intermediate level "*" by solving the advection–diffusion equations without the pressure gradient and the virtual force at the beginning of each time step. This step is implemented by the following formula:

$$\frac{\mathbf{u}^* - \mathbf{u}^m}{\Delta t} = S^m, \tag{11}$$

where S^m includes the convective and diffusive terms in Eq. (2).

The intermediate velocity $\mathbf{u}^*$ in Eq. (2) does not satisfy the continuity equation (1). At the second step, $\mathbf{u}^*$ is marched to the second intermediate velocity $\mathbf{u}^{**}$ by including the pressure gradient term

$$\frac{\mathbf{u}^{**} - \mathbf{u}^*}{\Delta t} = -\nabla p^{m+1}. \tag{12}$$

Taking the divergence of Eq. (12) gives

$$\frac{\nabla \cdot \mathbf{u}^{**} - \nabla \cdot \mathbf{u}^*}{\Delta t} = -\nabla^2 p^{m+1}, \tag{13}$$

which is solved by the SOLA algorithm proposed by Hirt et al. (1975). Furthermore, we update the velocity to the $(m+1)$th time level by imposing the virtual force term as follows:

$$\eta\frac{\mathbf{u}^{m+1} - \mathbf{u}^{**}}{\Delta t} = \mathbf{f}^{m+1}. \tag{14}$$

The virtual force term, $\mathbf{f}^{m+1}$, in Eq. (14) reveals the existence of a force to hold or to drive a solid body when it is stationary or moving. To satisfy the no-slip boundary condition for the solid motion, the force acting on the solid should make sure that the fluid velocity $\mathbf{u}$ is equal to the solid velocity $\mathbf{u}_s$ at the $(m+1)$th time step, i.e., $\mathbf{u}^{m+1} = \mathbf{u}_s^{m+1}$. Therefore, the virtual force is defined as the rate of momentum changes of solid body and proportional to the difference between the solid velocity at the $(m+1)$th time step and the fluid velocity at the mth time step. The force exists at the fluid domain where the solid body is immersed and zero elsewhere. Furthermore, it can be simply written as

$$\mathbf{f}^{m+1} = \eta\frac{\mathbf{u}^{m+1} - \mathbf{u}^{**}}{\Delta t} = \eta\frac{\mathbf{u}_s^{m+1} - \mathbf{u}^{**}}{\Delta t}. \tag{15}$$

The cylinders are stationary, so $\mathbf{u}_s$ is always zero for all cylinders in simulations.

The finite volume method is used to solve the momentum equations in this study. The advective scheme is discretized by the third QUICK scheme. The Adams–Bashforth scheme is used to solve the temporal derivative. Nonuniform grids are utilized as shown in Fig. 2. The grid space is reduced toward a cylinder and determined by the following formula (Kuyper et al., 1993):

$$x_i = \frac{i}{i_{\max}} - \frac{k}{\theta}\sin\left(\frac{i\theta}{i_{\max}}\right), \tag{16}$$

for the ith node. The term $\theta = 2\pi$ stretches both ends of a domain whereas $\theta = \pi$ clusters more grids in one end of a domain. The term k varies between 0 and 1. As k approaches 1 more grids are clustered near the end. Moreover, uniform grids are used in the tight area adjacent to a cylinder. There are 250×220 and 430×430 grids used for a single cylinder and four cylinders, respectively. The tight area adjacent to a cylinder adopts $\Delta x = \Delta y = 0.028$. The time increment $\Delta t = 10^{-4}$ satisfies the CFL condition. The convergence criterion $\mathcal{D} = 10^{-4}$ for the maximum mass residual is employed in this study. The total time of the simulation is 230. It takes more than 2 days for a simulation of 2-D oscillatory flow around a cylinder at a PC cluster consisting of AMD Athlon CPU 1913 MHz.

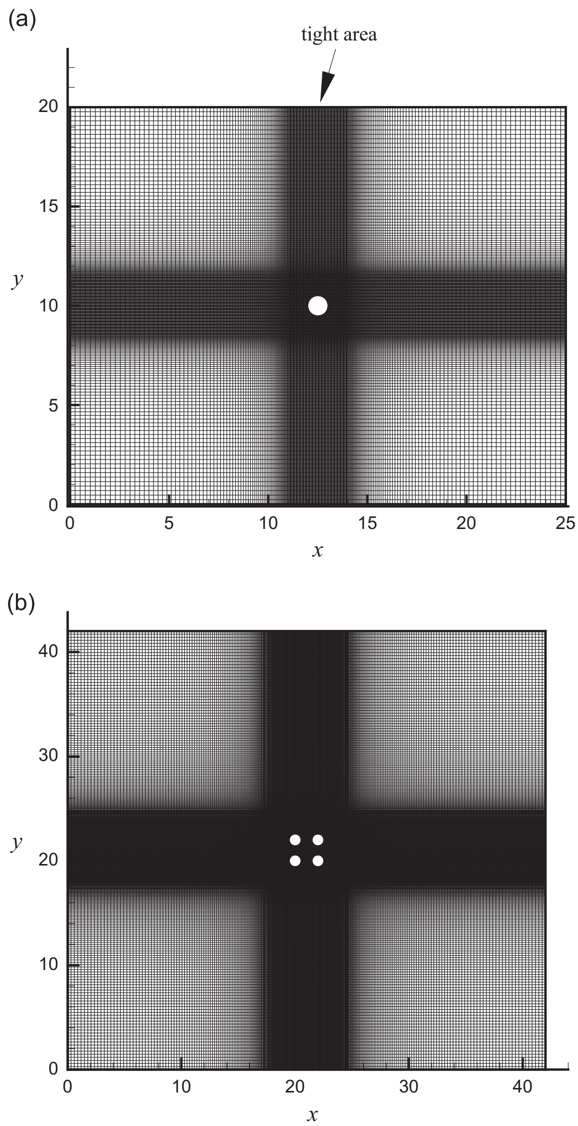

Fig. 2. Schematic of nonuniform grids with (a) a single circular cylinder, (b) four circular cylinders.

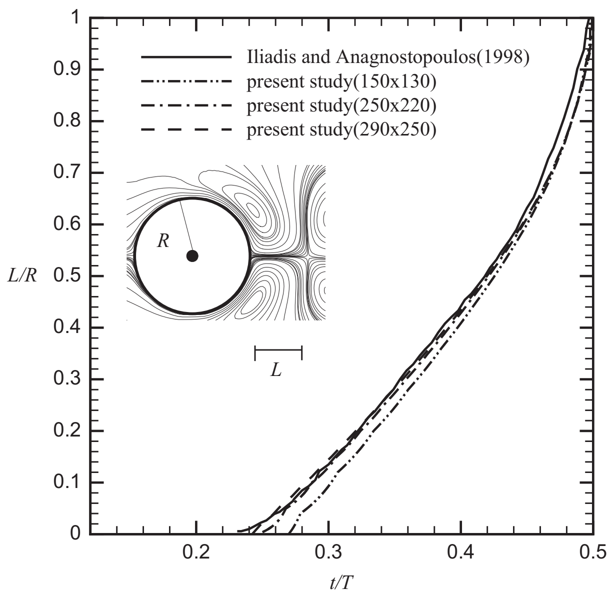

Fig. 3. Grid independence at KC=2 and Re=200.

2.5. Validation of the numerical model

2.5.1. Domain description and validation method

Fig. 1(a) shows the schematic of the benchmark test problem which is concerned with an oscillatory flow past a single cylinder. The computational domain is $25D \times 20D$. The cylinder is located in the middle of the computational domain. In order to validate the established numerical model, a comparison has been done with two cases involving numerical methods and one experimental case. Simulations are done for KC=2 and 10 and Re=200. The experimental data used for comparison was the variation of the root mean square value of in-line force with KC, for β=53.

2.5.2. Grid independence and validation

To show the grid independence in the numerical results, several grid systems are considered for oscillatory flow past a single cylinder at KC=2 and Re=200. The results are shown in Fig. 3. The wake is elongated as time marches. The predicted wake length in the model agrees with Iliadis and Anagnostopoulos (1998). The result from grids 250×220 is more accurate than that by 150×130. Also, as 250×220 grids are used, it takes less time than the case with 290×250 grids. Therefore, 250×220 grids are adopted for computation in this study. In addition, we compare the predicted in-line force C_f with other studies. Fig. 4(a) and (b) shows the time histories of C_f at KC=2 and 10. It is found that C_f will reach the maximum when the

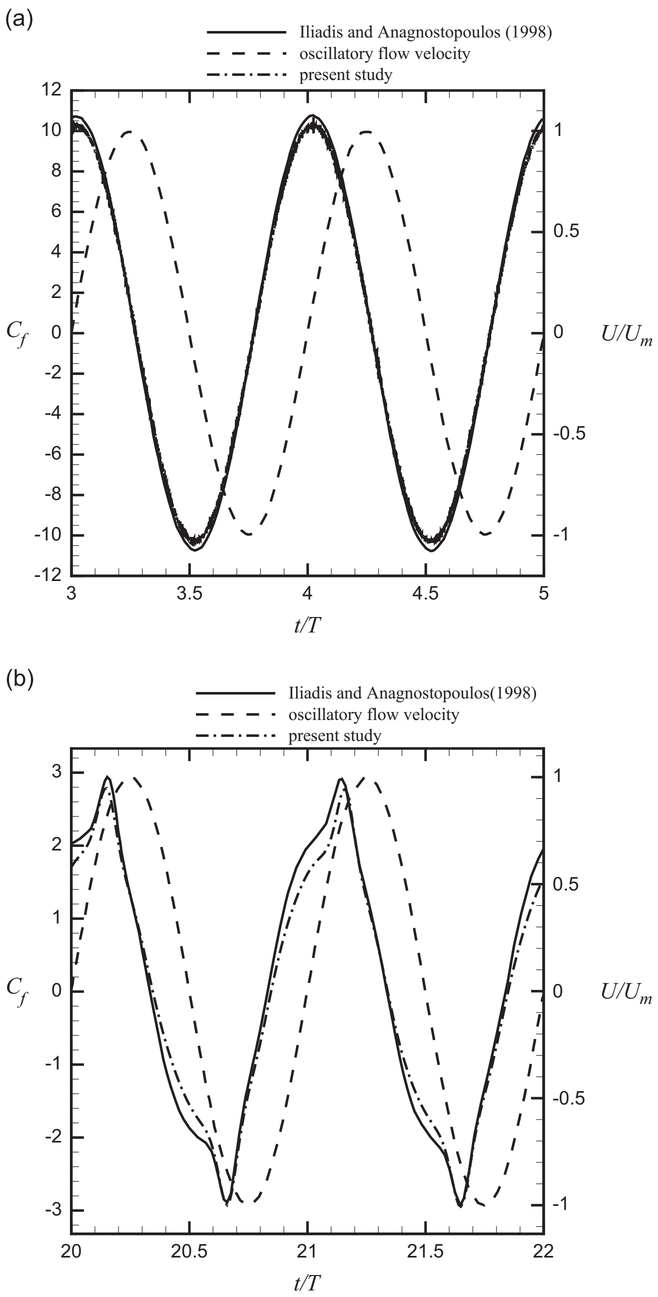

Fig. 4. Time histories of C_f at (a) KC=2, (b) KC=10.

oscillatory flow changes its direction and C_f decreases as the KC number increases. The results agree with those of the Iliadis and Anagnostopoulos (1998) study. Subsequently, the root mean square value of C_f is compared with experimental evidence by Kuhtz (1996) in Fig. 5. It shows a good agreement between computed and measured values. Those two test results show that the established model is able to simulate the interaction of oscillatory flow with a single cylinder and prediction of hydrodynamic loading is reasonable.

3. Results and discussion

The schematic of the oscillatory flow past a circular cylinder array in a square arrangement is shown in Fig. 1(b). The distance between centers of two neighboring cylinders is denoted by P. The pitch ratio P/D is one of the parameters that

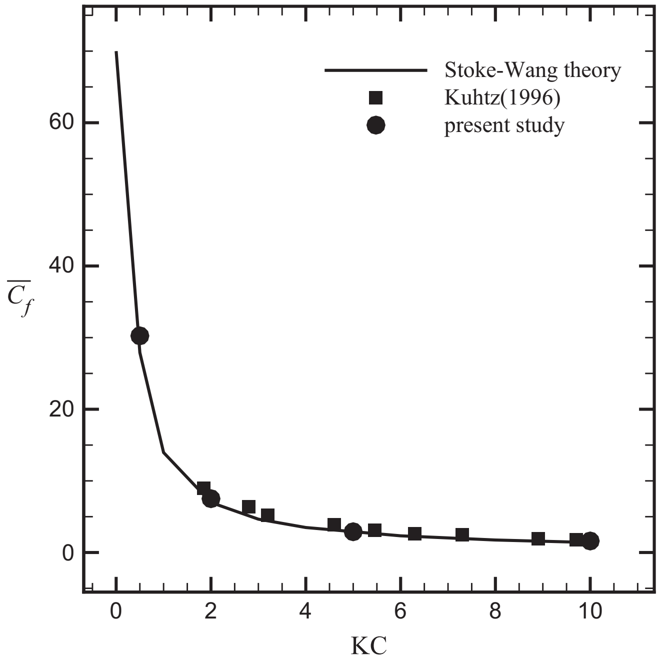

Fig. 5. Root mean square value of C_f as a function of KC for $\beta=53$.

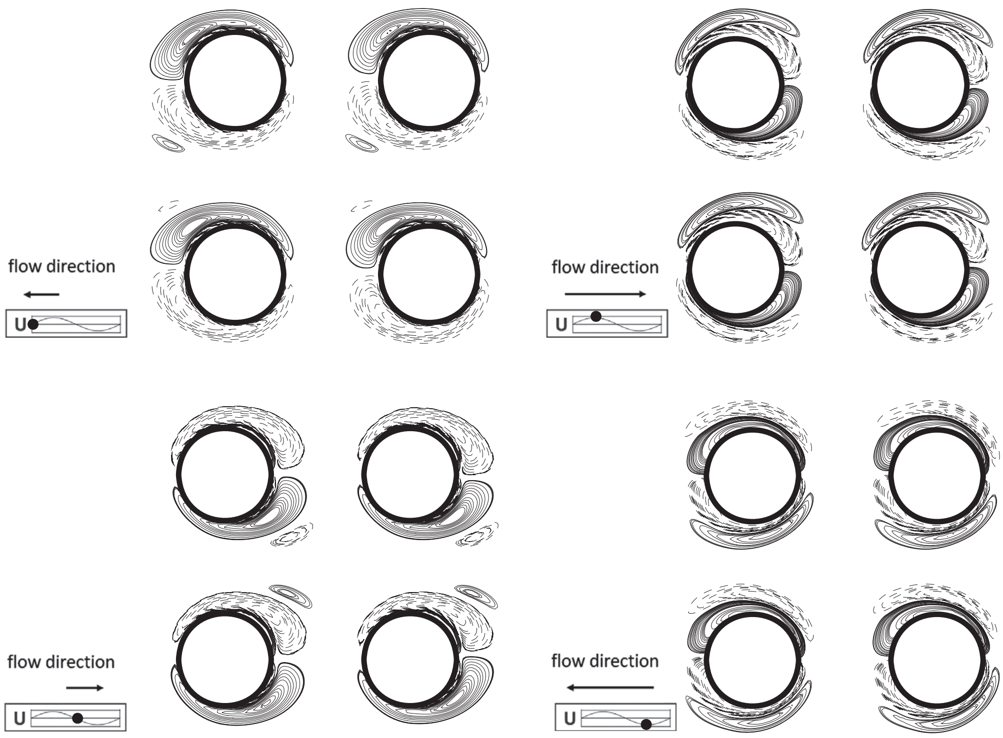

Fig. 6. Snapshots of vorticity contours in the horizontal oscillatory flow interacting with four cylinders during a cycle at KC=2, $P/D=2$ and $\beta=50$.

affect the hydrodynamic behavior around those cylinders. A variety of effects on the interaction of oscillatory flows with the cylinder array are demonstrated in the following sections.

3.1. Effect of KC number

A dimensionless parameter referred to KC number (U_mT/D) is used to express the stroke (U_mT) of the orbital motion of fluid particles in relation to the diameter (D) of the cylinder. A closer examination of the Navier–Stokes equation shows that

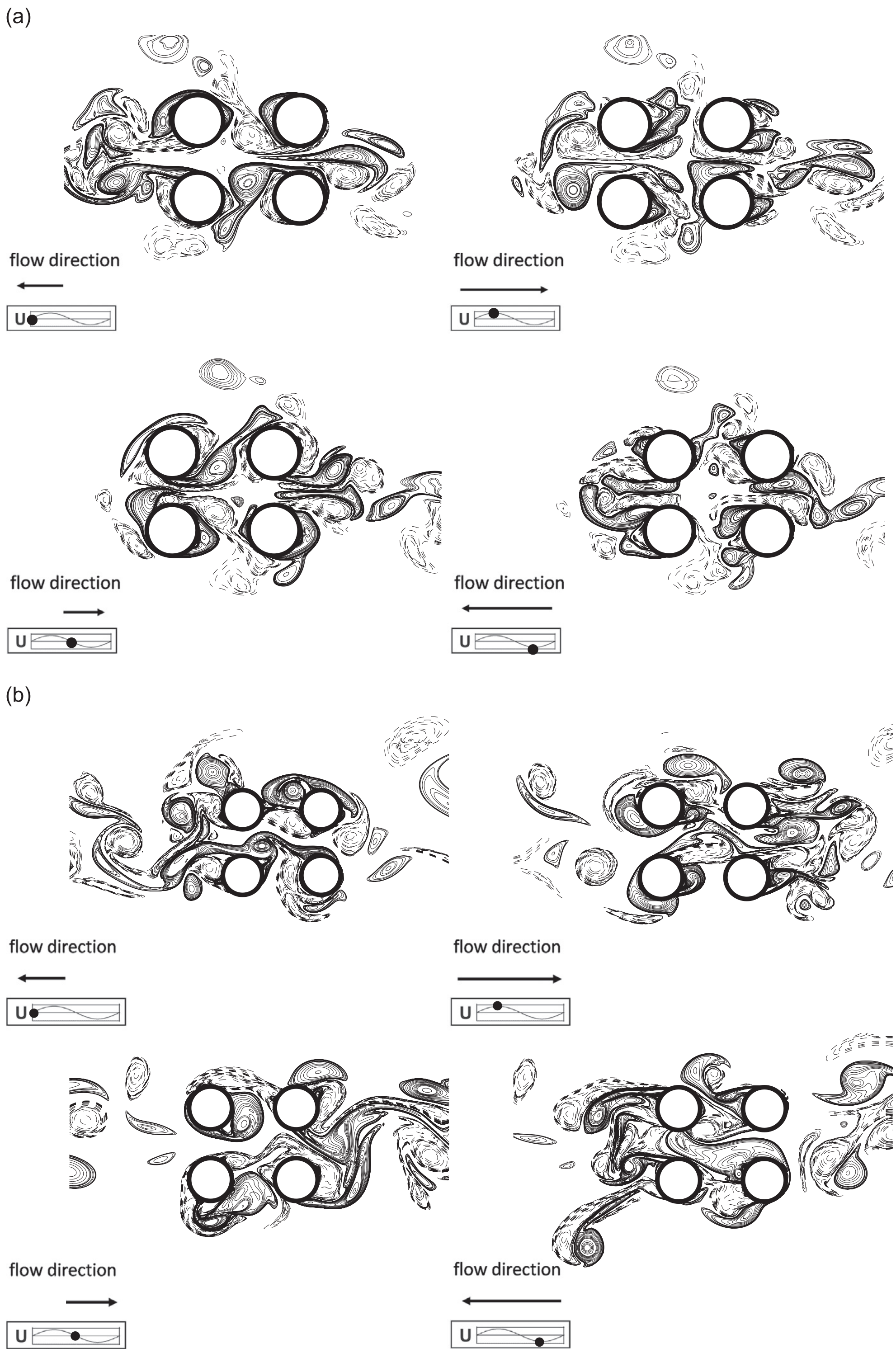

Fig. 7. Snapshots of vorticity contours in the horizontal oscillatory flow interacting with four cylinders during a cycle at (a) KC=5, (b) KC=10; $P/D=2$ and $\beta=50$.

the KC number can also be explained as the ratio of the convective to the unsteady force terms. In this regard, the ratio of the Reynolds to the KC numbers produces another dimensionless parameter known as β. Hence, β is a ratio of the unsteady to the viscous force terms in the Navier–Stokes equation. The physical relevance of β might be to identify the unsteady state regime of the oscillatory flow. In order to investigate the KC number effect on a horizontal oscillatory flow past a circular cylinder array at $P/D=2$ and $\beta=50$, KC varies from 2 to 40 in this study. The KC effect is explained in the following subsections.

3.1.1. *Flow patterns*

Fig. 6 shows the evolution of vorticity contours around four cylinders within a cycle at KC=2. The vortices occur alternatively in two sides and are attached on each cylinder. The flow pattern is symmetric with respect to the horizontal central line of the domain. Those vortical systems do not interact with each other. As KC number increases to 5, the vortices are no longer attached, having been shed from the cylinders. The vortices interact with others and the flow pattern becomes asymmetric as shown in Fig. 7(a). When the KC number is 10 as shown in Fig. 7(b), the vortical systems become more chaotic in comparison with the case at KC=5. Those vortices are not damped until they travel far away from cylinders.

3.1.2. *Variation of C_f with KC*

The in-line force coefficient C_f is an important physical quantity in an oscillatory flow field. The results are compared using a variety of KC numbers to simulate an oscillatory flow past a circular cylinder array. Fig. 8 demonstrates the time histories of C_f on the first cylinder. The maximum occurs at KC=2 in Fig. 8(a) and C_f behaves sinusoidally. It is similar to the single cylinder case. As KC increases to 5, the sinusoidal form of C_f is not regular any more as shown in Fig. 8(b). When KC is

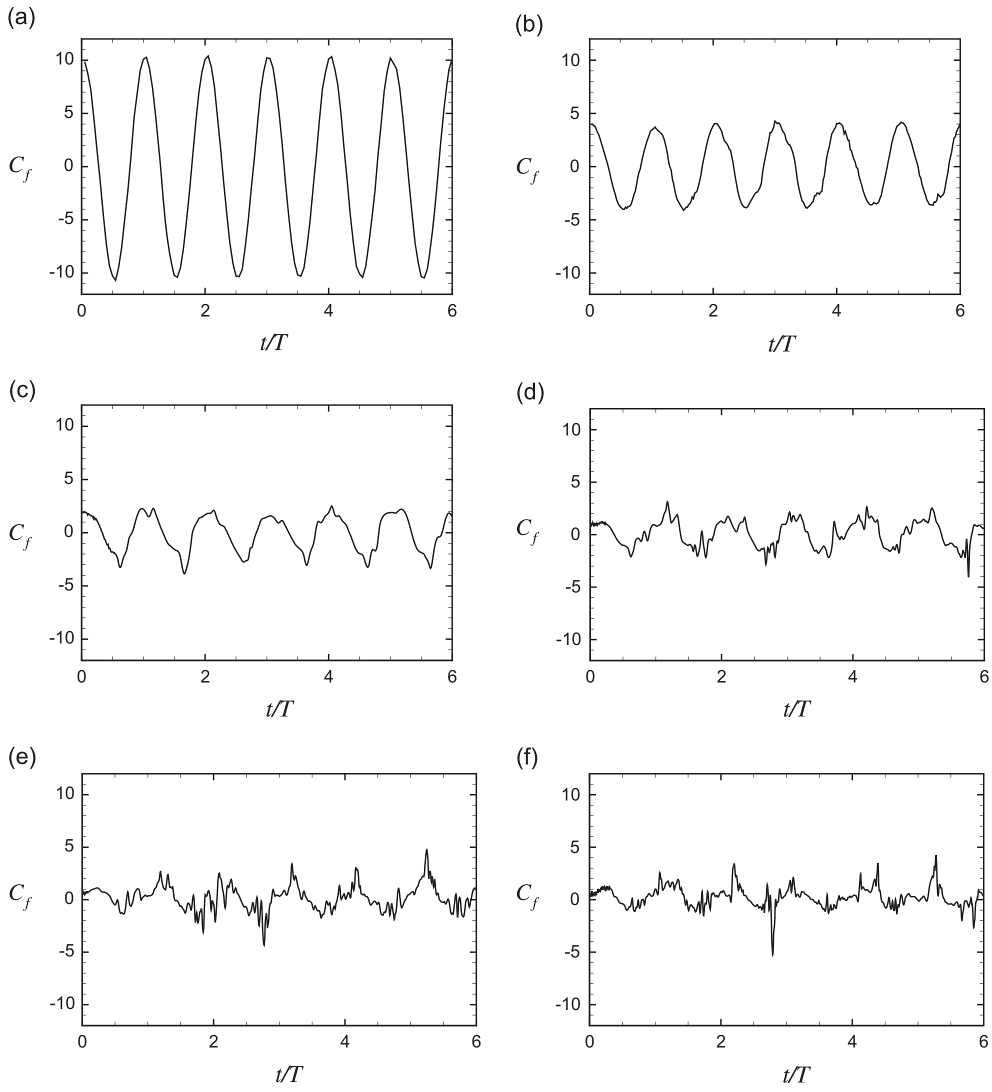

Fig. 8. Time histories of C_f of the first cylinder at (a) KC=2, (b) KC=5, (c) KC=10, (d) KC=20, (e) KC=30, (f) KC=40; $P/D=2$ and $\beta=50$.

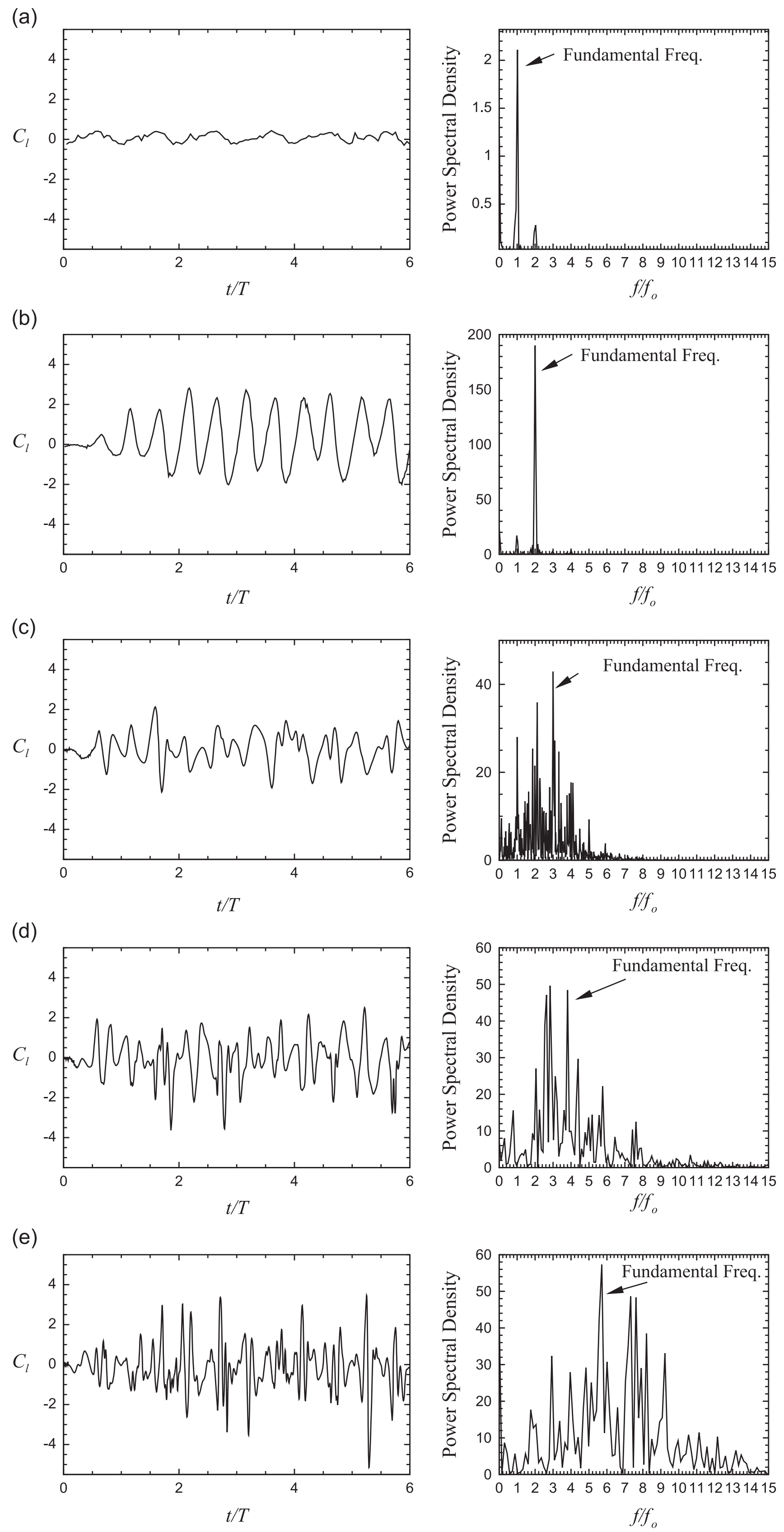

Fig. 9. Time histories of C_l of the first cylinder and spectrum analysis at (a) KC=2, (b) KC=5, (c) KC=10, (d) KC=20, (e) KC=30, (f) KC=40; $P/D=2$ and $\beta=50$. f_o is the frequency of the oscillatory flow.

raised to 10, the amplitude of C_f fluctuates intensely and the amplitude of C_f decreases again. For high KC numbers varying from 20 to 40, C_f is smaller than those at KC=2, 5 and 10. The value of C_f does not vary significantly at high KC. As KC number increases, it is found that the decrease of C_f is similar to the case of a single cylinder (Fig. 5). The influence of the vortices on the cylinders is more pronounced and the vortices travel farther from the cylinders due to the induced velocity effect.

3.1.3. Variation of C_l with KC

Fig. 9 depicts the time histories of C_l on the first cylinder and their spectrum analysis for various KC numbers. When KC is 2 in Fig. 9(a), the vortices are attached to each cylinder and the flow pattern is symmetric with respect to the horizontal

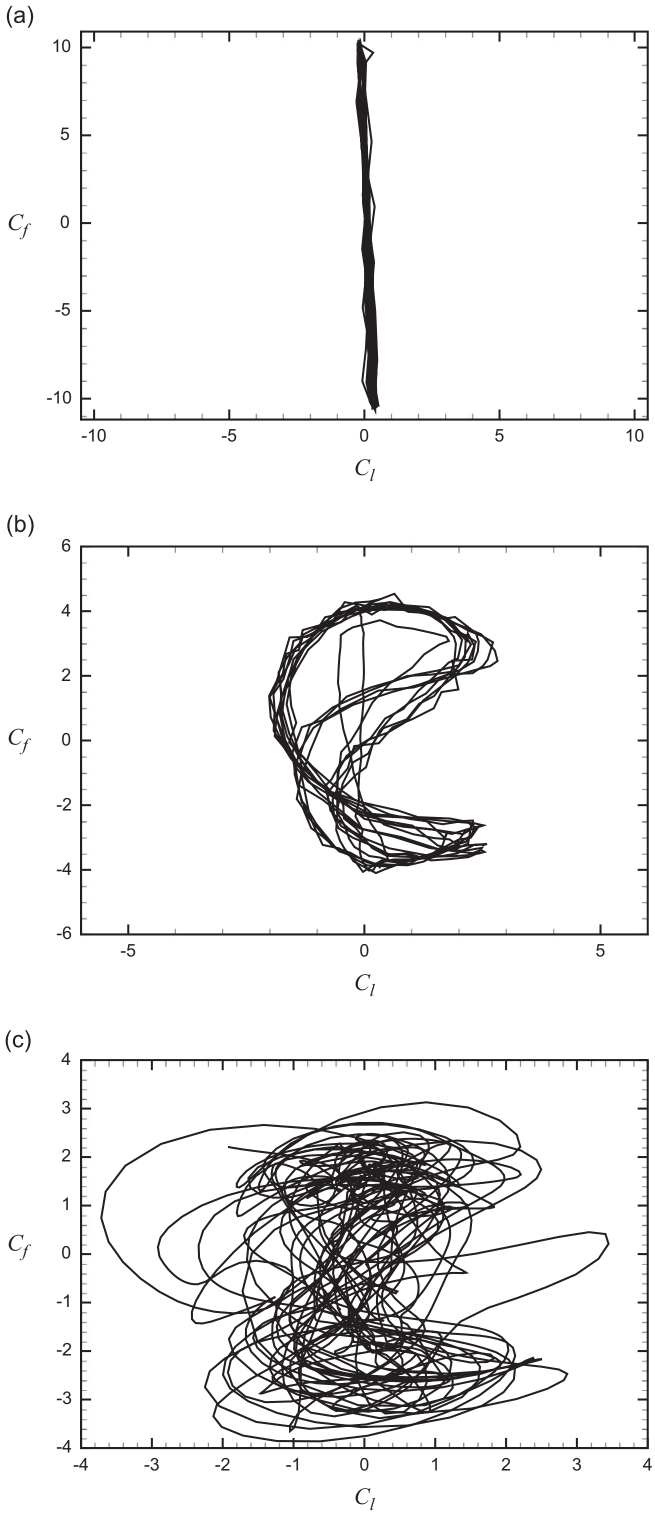

Fig. 10. Phase diagrams of C_f versus C_l of the first cylinder at (a) KC=2, (b) KC=5, (c) KC=10.

central line of the domain. According to the spectral analysis of C_l, the ratio of fundamental frequency of C_l to the frequency of the oscillatory flow is 1. This means that the fundamental frequency of C_l and that of the oscillatory flow are equal. That is, the variation of C_l is only dominated by the oscillatory flow. The absence of vortex shedding can be thought of as being the result of insufficient time required for shedding, since KC is only equal to 2. As KC increases to 5 in Fig. 9(b), C_l becomes

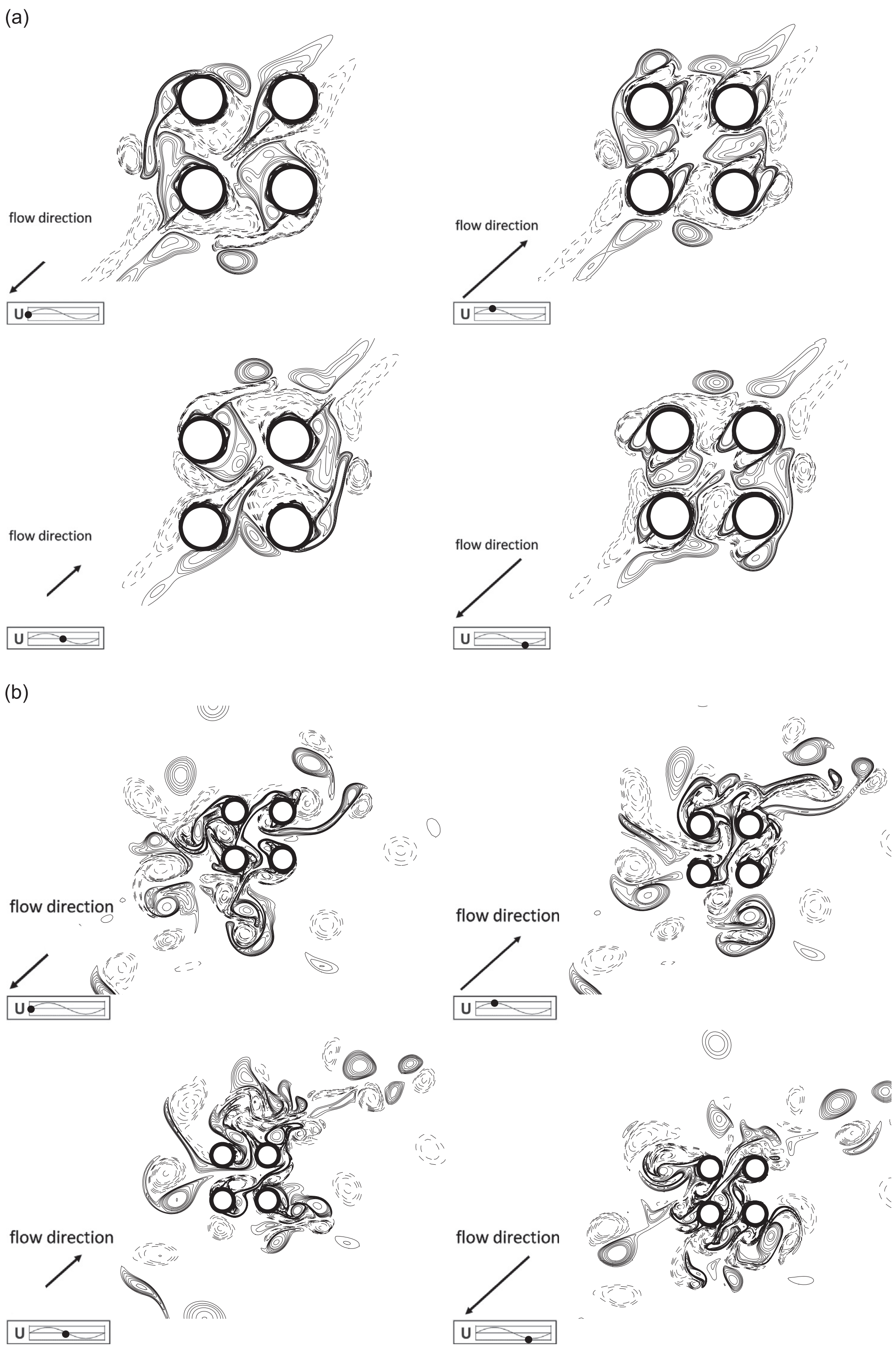

Fig. 11. Snapshots of vorticity contours in the oblique oscillatory flow interacting with four cylinders during a cycle at (a) KC=5, (b) KC=10; $P/D=2$ and $\beta=50$.

irregular and larger than the case at KC=2. The ratio of the fundamental frequency of C_l to that of the oscillatory flow shifts from 1 to 2. This jump in frequency is due to vortex shedding, which is made possible owing to sufficient time for the evolution of a pair of vortices, since KC is now larger. As KC increases to 10 in Fig. 9(c), the variation of C_l becomes faster and more irregular. The ratio of fundamental frequency of C_l to that of the oscillatory flow is 3 at KC=10. In high KC numbers, the ratio becomes 3.81 at KC=20, 5.70 at KC=30 and 6.71 at KC=40. Seemingly, a trend that suggests the increase of the fundamental frequency of C_l with an increase in KC exists. According to those results, more subharmonics appear in the spectrum analysis as KC increases. The appearance of the subharmonics is due to the difference in the vortex shedding and fluid oscillatory frequencies. This difference induces secondary frequencies. This is because more vortices occur at high KC numbers. Complex vortex motion excites more subharmonics in the spectrum of C_l. Therefore, when KC increases, it can be expected that more vortices are generated and more subharmonics appear in the spectrum. Also, the fundamental frequency of C_l becomes faster than the frequency of the oscillatory flow.

3.1.4. Phase diagram of C_f versus C_l

The hydrodynamic forces exerted on cylinders can be regarded as the responses of the vortical systems around those cylinders. The trajectories of C_f versus C_l at successive instants reveal the states of the vortical systems. Fig. 10 shows the phase diagram of C_f versus C_l of the first cylinder at various KC numbers. A case of zero lift occurs at KC=2 as shown in Fig. 10(a). The reason for such a trajectory is that the vortical system is symmetric at KC=2. Thus if C_l is very small then the trajectory will be almost periodic. As KC increases to 5, the vortices influence each other, leading to a larger value of C_l as compared with the case at KC=2. The trajectory resembles the number “8” as shown in Fig. 10(b). Moreover, the trajectory is

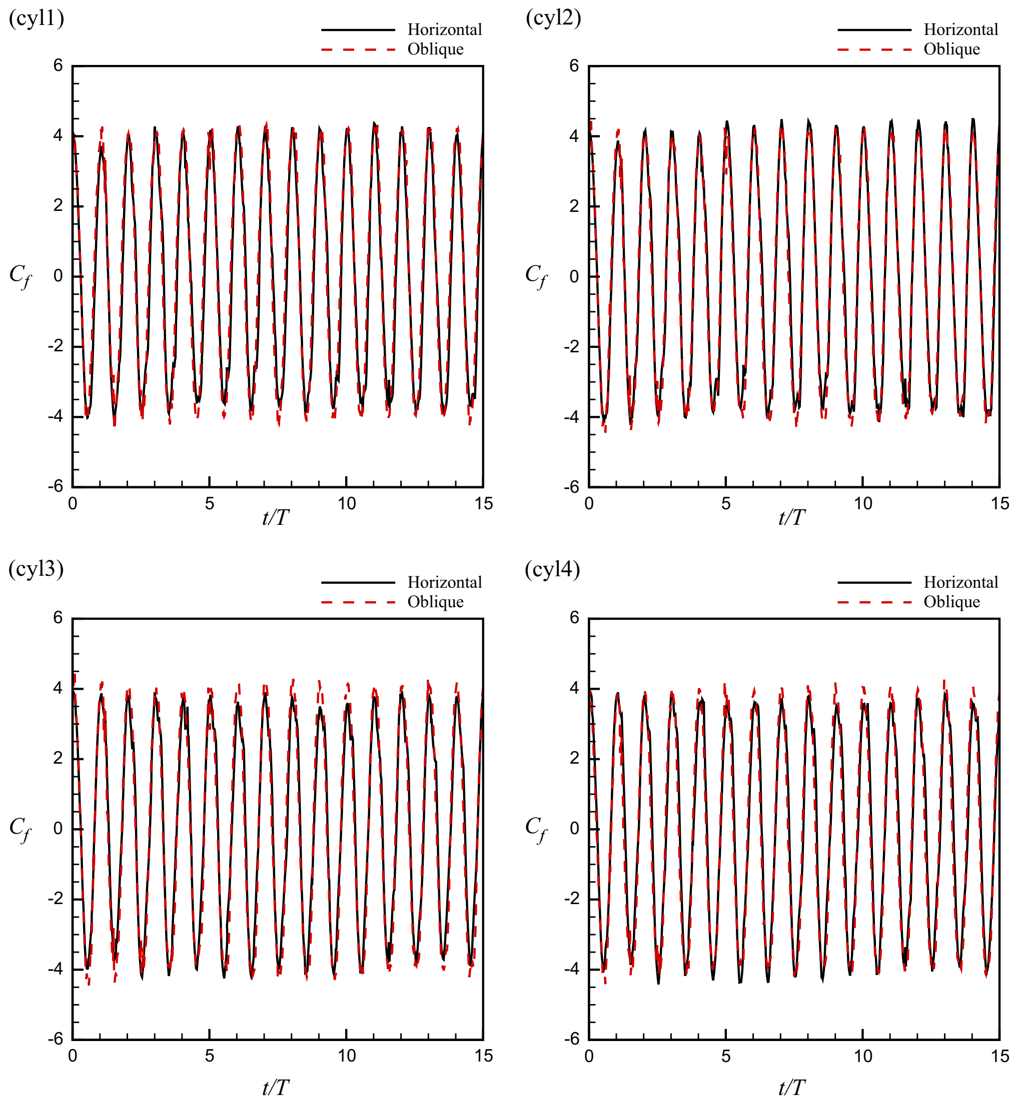

Fig. 12. Time histories of C_f of each cylinder in in-line and oblique oscillatory flows at KC=5, P/D=2 and β=50.

very chaotic when KC increases to 10 as shown in Fig. 10(c). The figures illustrate that the vortical system changes from a periodic to a chaotic state with increasing KC numbers.

3.2. Effect of oblique flow

We investigate a 45° oblique oscillatory flow past a circular cylinder array at $P/D=2$ and $\beta=50$ in this section. Two KC values, 5 and 10, are considered. The effects of oblique flow on hydrodynamic loadings and flow patterns are discussed.

3.2.1. Flow patterns

Fig. 11 shows the evolution of vorticity contours around a circular cylinder array during a cycle. The flow pattern is symmetric with respect to the oblique diagonal line of the domain at KC=5 as shown in Fig. 11(a). All of the vortices occur in alternating sequence on different sides of those cylinders. This result is different from an in-line oscillatory flow past those cylinders at KC=5, since the vorticity contours in the in-line flow are asymmetric. The symmetry in those vortical systems vanishes as KC is increased to 10 as shown in Fig. 11(b). The vortices are shed from the cylinders downstream and the travel distance is longer than that at KC=5. In general, the vortical system becomes irregular as KC changes from 5 to 10.

3.2.2. Variations of C_f in in-line and oblique oscillatory flows

In order to investigate the effect of the angle of attack between the oscillatory flow and the in-line axis of the cylinder array, the hydrodynamic loadings in the in-line and oblique flows are compared. The values of C_f on each cylinder in the

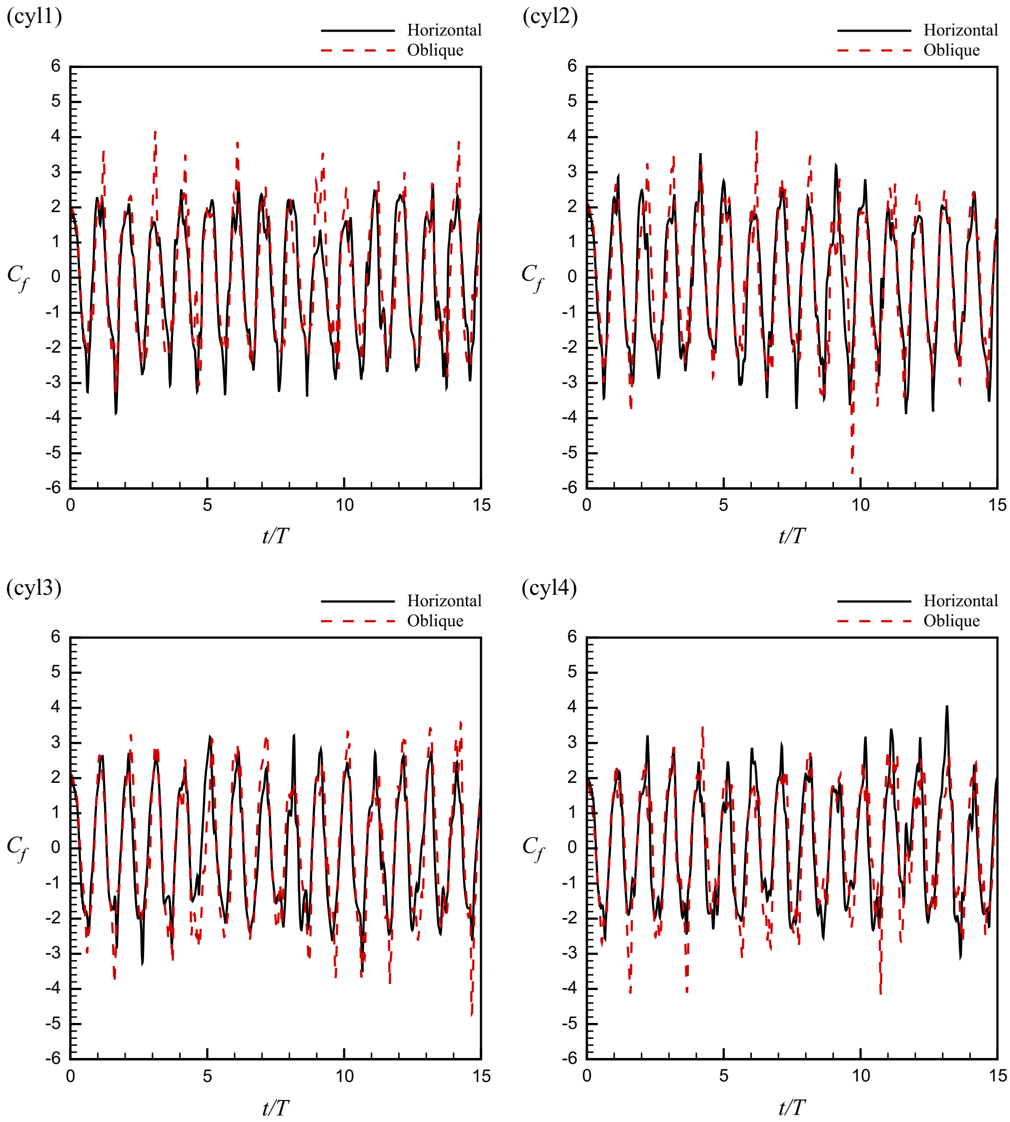

Fig. 13. Time histories of C_f of each cylinder in in-line and oblique oscillatory flows at KC=10, $P/D=2$ and $\beta=50$.

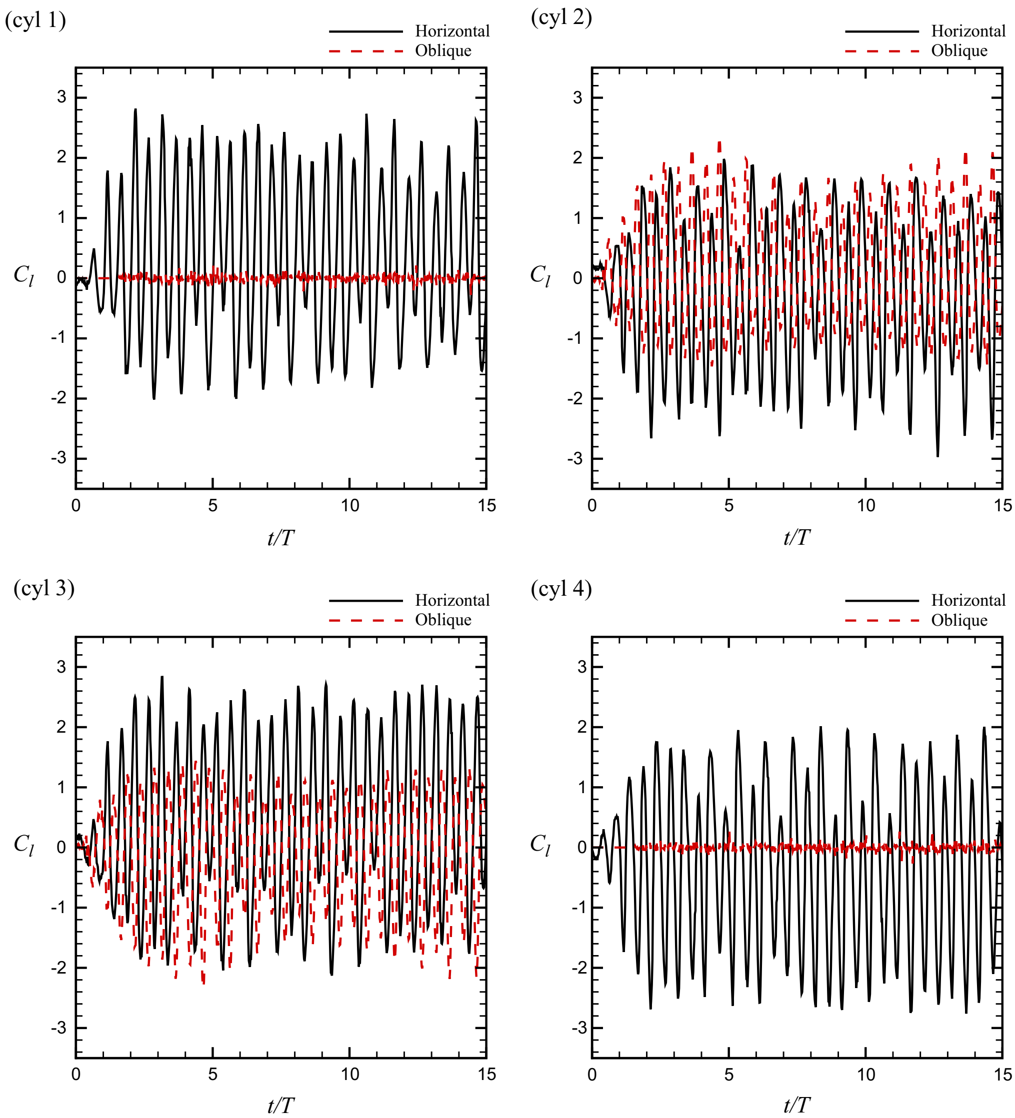

Fig. 14. Time histories of C_l of each cylinder in in-line and oblique oscillatory flows at KC=5, $P/D=2$ and $\beta=50$.

oblique flow are almost the same as those results in the horizontal flow at KC=5, as shown in Fig. 12. The amplitude of C_f fluctuates intensely, C_f is slightly larger than the in-line flow case in Fig. 13, when KC number increases to 10.

3.2.3. *Variations of C_l in in-line and oblique oscillatory flows*

Fig. 14 shows that C_l on all the cylinders in the oblique flow is smaller than that in the in-line flow at KC=5 due to the flow patterns which are symmetric with the oblique diagonal line of the domain at KC=5. In particular, values of C_l on the first and the fourth cylinder have minimal fluctuation in the oblique flow. The values of C_l for the second and the third cylinder are significantly different compared to the values of the first and the fourth cylinder. Nevertheless, the results at KC=10 as shown in Fig. 15 are contrary. As KC increases to 10, the flow patterns change from symmetric to asymmetric as time marches. The values of C_l on all the cylinders in the oblique flow are larger than those in the in-line flow. According to the spectral analysis of C_l on the second and the third cylinder, the ratios of fundamental frequency of C_l to the frequency of the oscillatory flow are 2 at KC=5 and 2.7 at KC=10. In the oblique flow, it has the same trend that the fundamental frequency of C_l increases with increasing KC.

3.2.4. *Comparison of the $\overline{C}_f$ and $\overline{C}_l$ with in-line flow*

The root mean square values of $\overline{C}_f$ and $\overline{C}_l$ in the horizontal and oblique flows are determined and shown in Table 1. Comparing the oblique and in-line flow directions, the values of $\overline{C}_f$ remain almost the same at the same KC number. The values of $\overline{C}_l$ do not have a significant trend. The value of $\overline{C}_l$ in the in-line oscillatory flow is larger than that in the oblique oscillatory flow at KC=5. At KC=10, $\overline{C}_l$ in the oblique oscillatory flow is larger than that in the in-line oscillatory flow. Moreover, in the oblique oscillatory flow, it is found that $\overline{C}_l$ on the second cylinder in the transverse flow direction is larger than that on the first cylinder in the in-line flow direction.

3.2.5. Phase diagram of C_f versus C_l

According to Fig. 16, it is evident that the trajectory has a regular pattern on each cylinder at KC=5. The trajectories of the first and the fourth cylinder are close to a straight line which is the same as the trajectories in the in-line oscillatory flow at

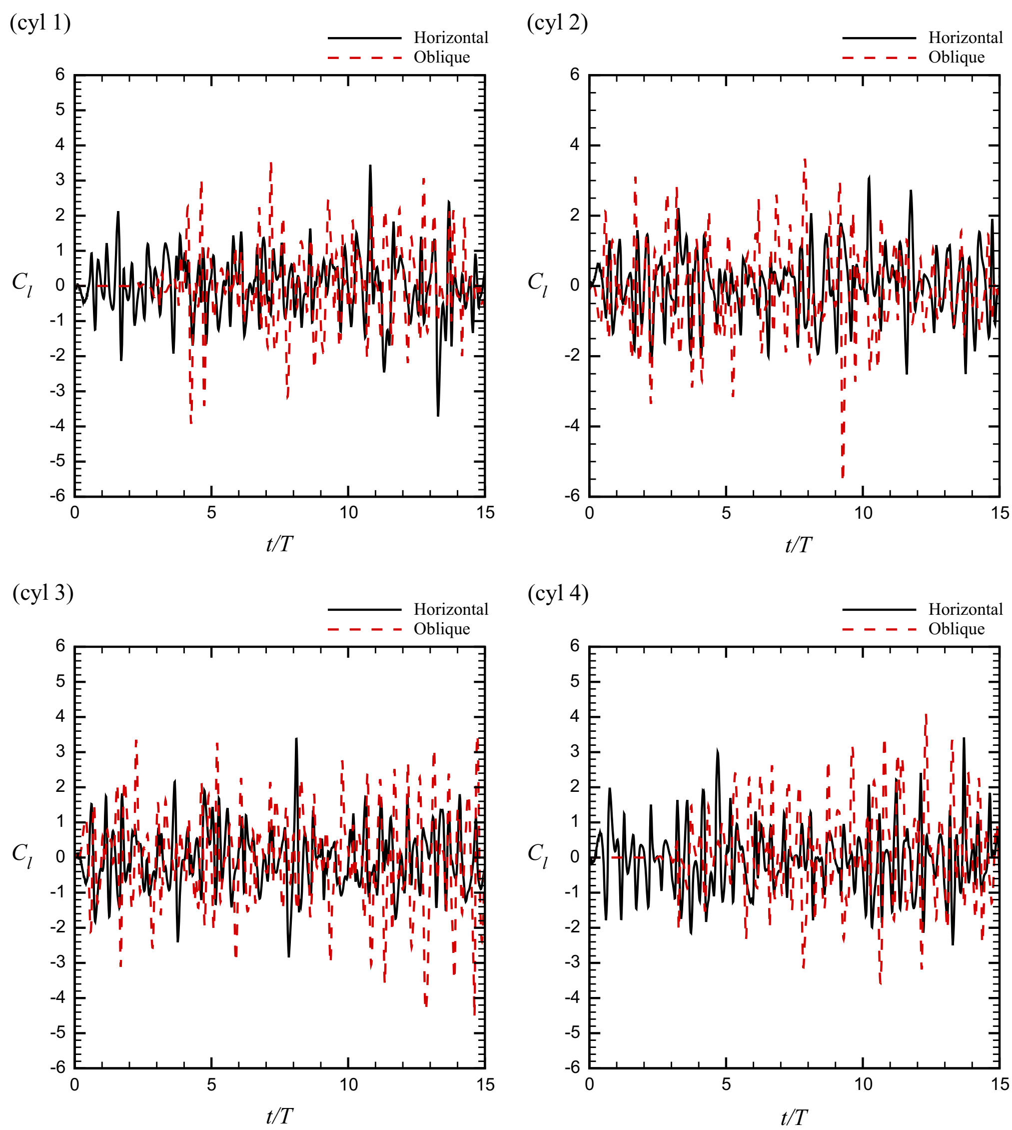

Fig. 15. Time histories of C_l of each cylinder in in-line and oblique oscillatory flows at KC=10, P/D=2 and β=50.

Table 1
Variation of $\overline{C}_f$ and $\overline{C}_l$ with respect to KC at β=50.

Flow direction	KC number	$\overline{C}_f$	$\overline{C}_l$
Horizontal (cyl 1)	KC=2	7.510	0.245
	KC=5	2.828	1.313
	KC=10	1.687	0.906
Oblique (cyl 1)	KC=2	7.152	0.050
	KC=5	3.003	0.053
	KC=10	1.719	0.983
Oblique (cyl 2)	KC=2	7.740	0.219
	KC=5	3.006	0.981
	KC=10	1.817	1.183

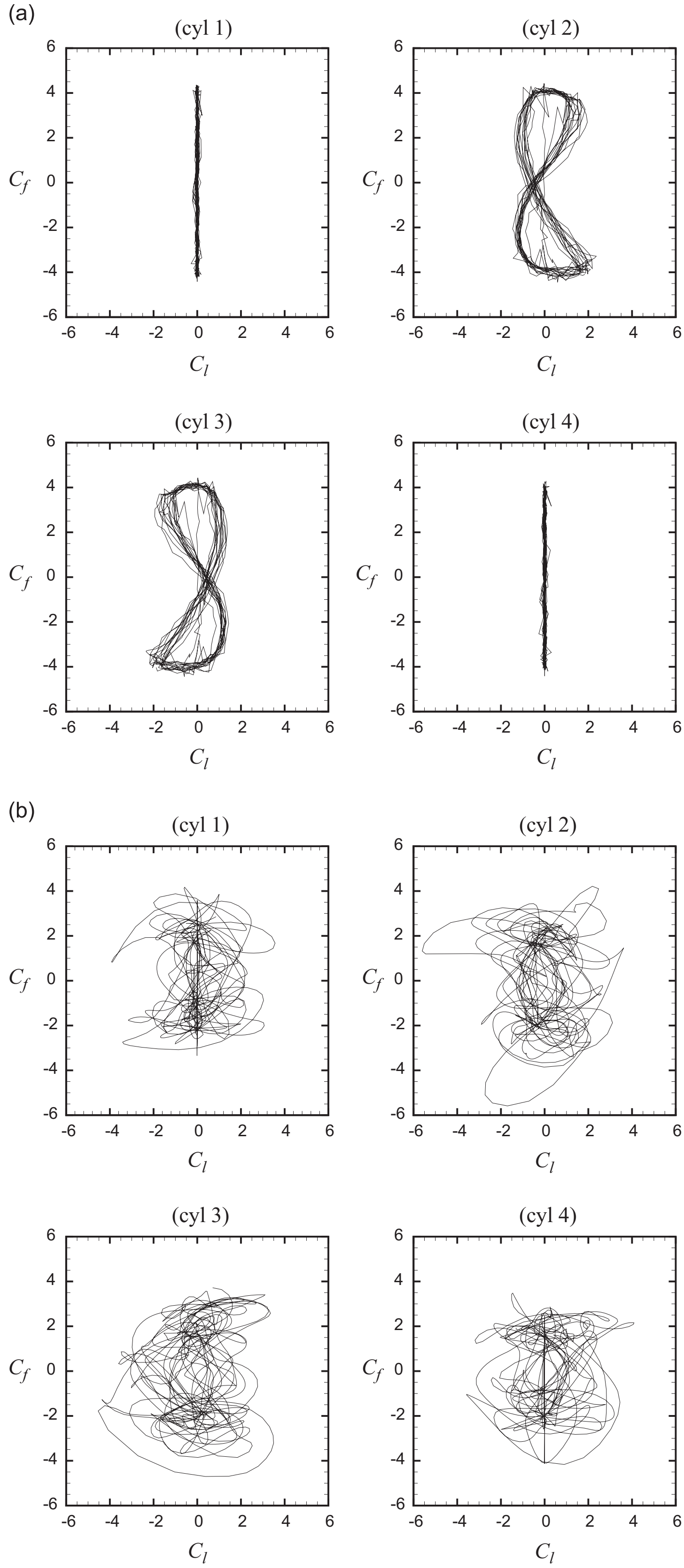

Fig. 16. Phase diagrams of C_f versus C_l of cylinders at (a) KC=5, (b) KC=10.

KC=2. The trajectories of the second and the third cylinders look like the number “8”. They are similar to the trajectories in the horizontal flow. Nevertheless, when KC increases to 10, the vortical system becomes chaotic, so the trajectories of all the cylinders become very disordered and unpredictable.

3.3. Effect of pitch ratio

The pitch ratio P/D is one of the important factors when a cylinder array is designed in an offshore platform. In order to investigate the pitch ratio effect on an in-line oscillatory flow past a circular cylinder array at KC=5 and 10 and β=50, four various pitch ratios 2, 3, 4 and 5 are considered.

Fig. 17 shows the time histories of C_f exerted on the first cylinder with a variety of pitch ratios at KC=5 and 10. It seems that C_f does not change at KC=5 when P/D varies. It is because the flow patterns are symmetric with respect to the in-line flow direction in those P/D values. The flow patterns are no longer symmetric and affected by P/D at KC=10, so the values of C_f are different when P/D varies. Fig. 18 shows the time histories of C_l exerted on the first cylinder, with different pitch ratios at KC=5 and 10. Their spectrum analysis of C_l is also illustrated. The value of C_l reaches a maximum at P/D=2 and becomes smaller when P/D is larger than 2. According to the spectrum analysis of C_l, the fundamental harmonic has the maximum at P/D=2 and becomes smaller when P/D gets larger than 2. The ratio of the fundamental frequency of C_l to the oscillatory flow

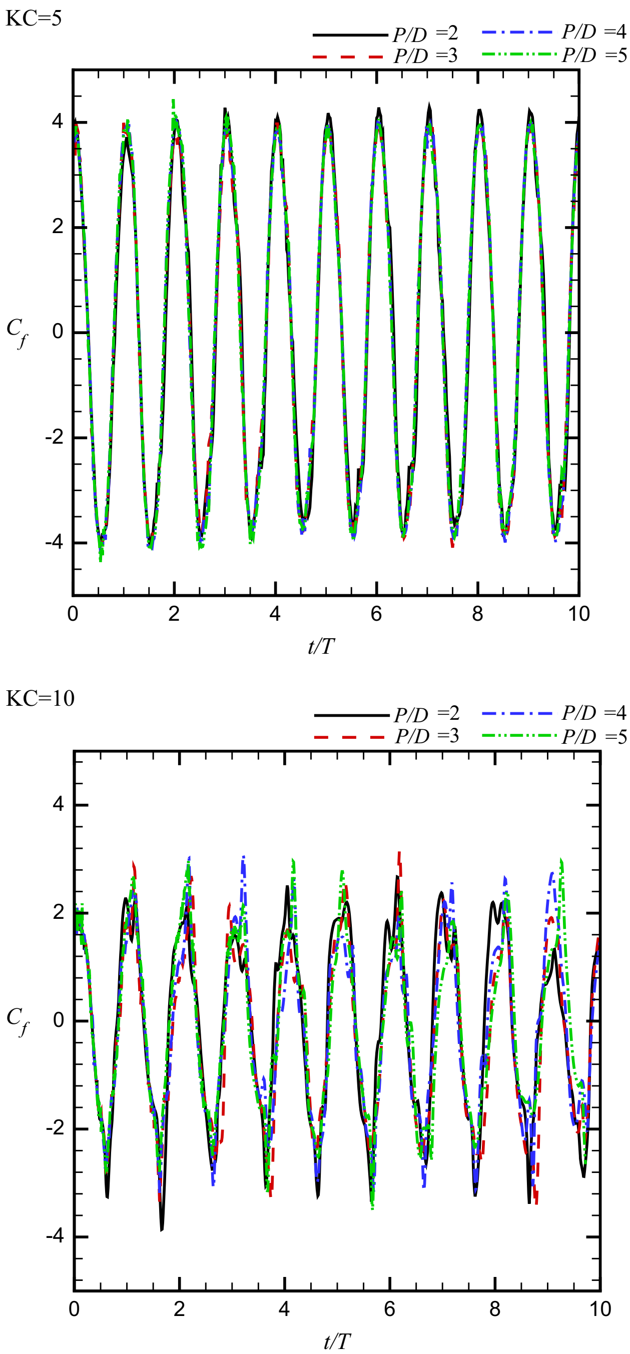

Fig. 17. Time histories of C_f of the first cylinder at different P/D, KC=5, 10 and β=50.

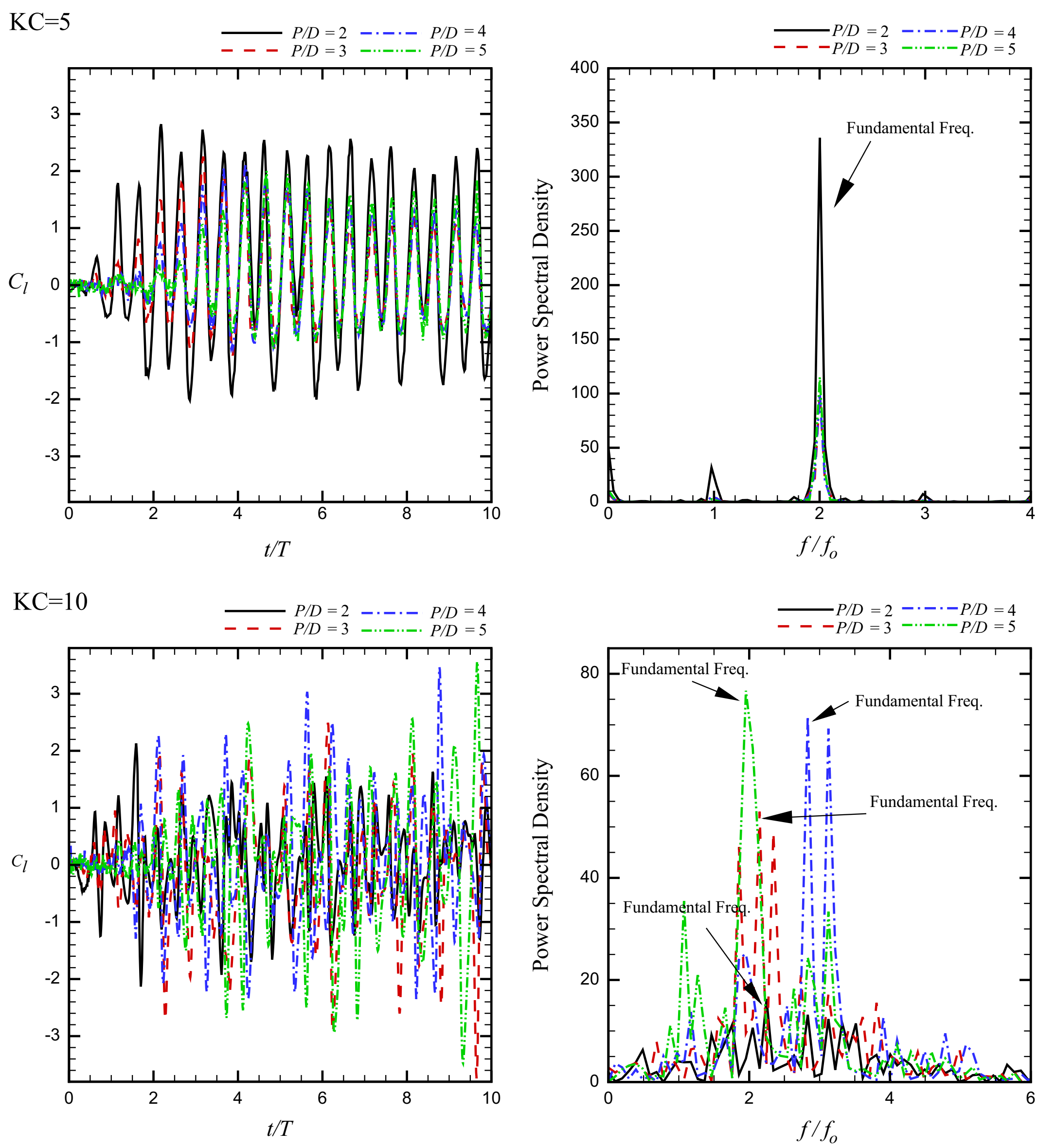

Fig. 18. Time histories of C_l and spectrum analysis of the first cylinder at different P/D, KC=5, 10 and β=50.

frequency for different P/D is 2. However, the results are contrary at KC=10 as shown in Fig. 18. The value of C_l is a minimum at $P/D=2$ and the magnitude of C_l becomes larger as P/D increases. The fundamental harmonic has a minimum at $P/D=2$ in the spectrum and becomes larger as P/D increases. The magnification of C_l is delayed with the increase of P/D. The results show that C_f is almost the same as P/D increases, but C_l, or its fundamental frequency, varies as P/D increases. The root mean square values of $\overline{C}_f$ and $\overline{C}_l$ for different P/D are compared and shown in Fig. 19. The result is in agreement with previous studies by Anagnostopoulos and Dikarou (2011). In their work, for all P/D cases, $\overline{C}_f$ decreases as KC increases and is almost fixed at each P/D for the same KC number. The value of $\overline{C}_l$ is larger at $P/D=2$ when KC is smaller than 5. However, $\overline{C}_l$ does not have a trend for increasing P/D when KC is larger than 5.

4. Conclusions

The present study has numerically investigated an oscillatory flow past a circular cylinder array to predict the hydrodynamic force on those cylinders. The direct-forcing immersed boundary method has been adopted to handle complex configurations of four cylinders in the Cartesian coordinates. The validation exercise has yielded positive results, most of which are in good agreement with the collected numerical and experimental data. The proposed direct-forcing immersed boundary model was validated by an oscillating flow interacting with a single cylinder at KC=2 and 10. The established numerical model was further applied to simulate oscillatory flows around four cylinders in a square arrangement at different conditions. There are three features that have been examined in this study. These are the effects of (i) increasing KC number, (ii) oblique angle, and (iii) pitch ratio.

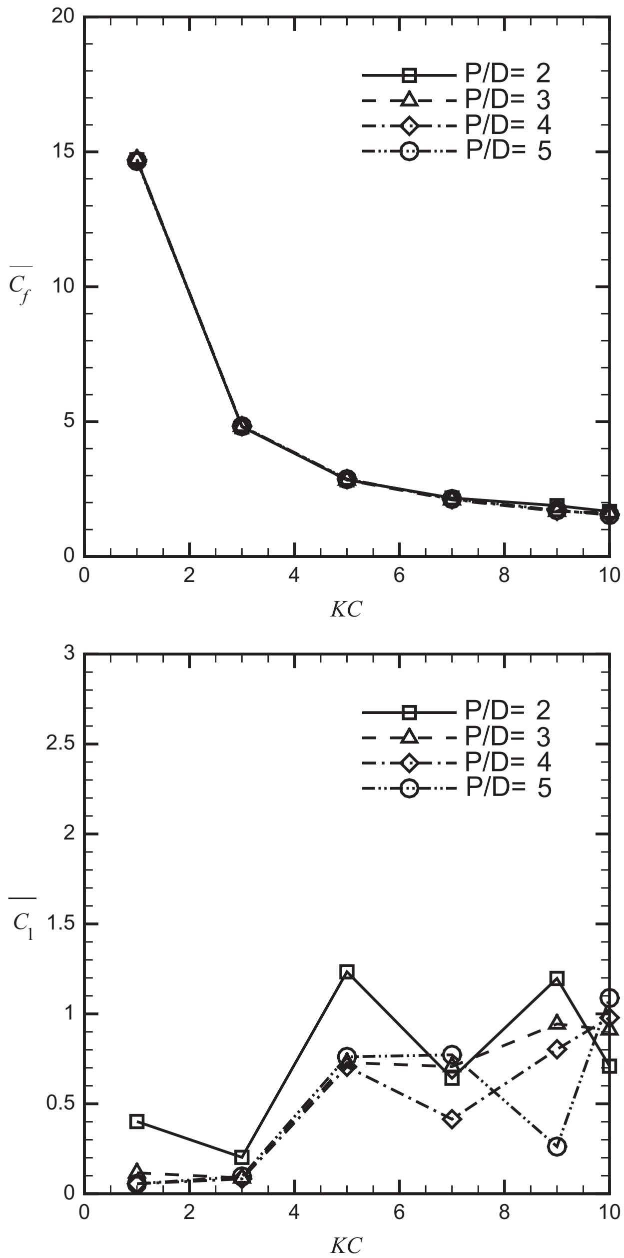

Fig. 19. $\overline{C}_f$ and $\overline{C}_l$ versus KC for the different pitch ratios examined at $\beta=50$.

The analysis for increasing KC numbers shows that more vortices occur at high KC numbers. The vortical systems become more chaotic and the vortices travel far away from the cylinders. Consequently, more vortices are generated and more subharmonics appear in the corresponding spectrum of lift coefficient C_l. It is also noted that the root mean square value of in-line force coefficient C_f is inversely proportional to KC. The fundamental frequency of C_l becomes faster and more subharmonics are excited as KC increases. The interaction of vortices results in a situation where the fundamental frequency of C_l overrides that of the oscillatory flow.

In order to investigate the effect of the oblique flow, the oscillatory flow direction becomes parallel to the diagonal axis of the cylinder array. The flow pattern is symmetric at KC=5. This result is different from an in-line flow past those cylinders. The comparison of C_f and C_l with the in-line and oblique oscillatory flows shows that C_f is not affected by the flow direction, while C_l becomes smaller at KC=5. In particular, the C_l values on the first and the fourth cylinder have minimal fluctuation in the oblique flow, but C_l becomes larger at KC=10. Moreover, in the oblique oscillatory flow, it is found that C_l on the second and the third cylinder is larger than that on the first and the fourth cylinders.

In addition, the effect of pitch ratio P/D is investigated. The results show that C_f is not affected by the pitch ratio. When KC is smaller than 5, C_l reaches the maximum at $P/D=2$ but remains at the same value for increasing P/D. As P/D increases, the predicted flow fields become close to the interaction of an oscillatory flow past a single circular cylinder.

Acknowledgments

The authors would like to express their gratitude for the financial support from National Science Council, Taiwan (Grant no. NSC 101-2212-E-011-043).

References

Anagnostopoulos, P., Minear, R., 2004. Blockage effect of oscillatory flow past a fixed cylinder. Applied Ocean Research 26, 147–153.
Anagnostopoulos, P., Dikarou, C., 2011. Numerical simulation of viscous oscillatory flow past four cylinders in square arrangement. Journal of Fluids and Structures 27, 212–232.
An, H., Cheng, L., Zhao, M., Dong, G., 2006. Numerical simulation of the oscillatory flow around two cylinders in tandem. Journal of Hydrodynamics 1, 191–197.
An, E., Cheng, L., Zhao, M., 2011. Direct numerical simulation of oscillatory flow around a circular cylinder at low Keulegan–Carpenter number. Journal of Fluid Mechanics 666, 77–103.
Chern, M.J., Rajesh Kanna, P., Lu, Y.J., Cheng, I.C., 2010. A CFD study of the interaction of oscillatory flows with a pair of side-by-side cylinders. Journal of Fluids and Structures 26, 626–643.
Fadlun, E.A., Verzicco, R., Orlandi, P., Yusof, J.M., 2000. Combined immersed-boundary finite-difference methods for three-dimensional complex flow simulation. Journal of Computational Physics 161, 35–60.
Hirt, C.W., Nichols, B.D., Romero, N.C., 1975. SOLA—A Numerical Solution Algorithm for Transient Fluid Flow. LA-5852 Technical Report. Los Alamos Scientific Laboratory, USA.
Iliadis, I., Anagnostopoulos, P., 1998. Viscous oscillatory flow around a circular cylinder at low Keulegan–Carpenter numbers and frequency parameters. International Journal of Numerical Methods for Numerical Methods in Fluids 26, 403–442.
Kuhtz, S., Bearman, P.W., Graham, J.M.R., 1997. Problems encountered in measuring forces on immersed bodies. Experimental Techniques 21, 20–23.
Kuhtz, S., 1996. Experimental investigation of oscillatory flow around circular cylinders at low beta numbers (Ph.D. thesis), Imperial College, UK.
Kuyper, R.A., van der Meer, T.H., Hoogendoorn, C.J., Henkes, R.A.W.M., 1993. Numerical study of laminar and turbulent natural convection in an inclined square cavity. International Journal of Heat and Mass Transfer 36, 2899–2911.
Lam, K., Zou, L., 2010. Three-dimensional numerical simulations of cross-flow around four cylinders in an in-line square configuration. Journal of Fluids and Structures 26, 482–502.
Langlee Wave Power, 2013 ⟨http://www.langleewavepower.com/⟩. accessed on 09/10/2013.
Noor, D.Z., Chern, M.J., Horng, T.L., 2009. An immersed boundary method to solve fluid–solid interaction problems. Computational Mechanics 44, 447–453.
Obasaju, E.D., Bearman, P.W., Graham, J.M.R., 1988. A study of forces, circulation and vortex patterns around a circular cylinder in oscillation flow. Journal of Fluid Mechanics 196, 467–494.
Peskin, C.S., 1973. Flow patterns around heart valves: a numerical method. Journal of Computational Physics 10, 252–271.
Sarpkaya, T., 1986. Force on a circular cylinder in viscous oscillatory flow at low Keulegan–Carpenter numbers. Journal of Fluid Mechanics 165, 61–71.
Su, S.W., Lai, M.C., Lin, C.A., 2007. An immersed boundary technique for simulating complex flows with rigid boundary. Computers and Fluids 36, 593–623.
Sumer, B., Fredosoe, J., 1997. Hydrodynamics Around Cylindrical Structures. World Scientific Publishing, Singapore (Chapter 3).
Suthon, P., Dalton, C., 2011. Streakline visualization of the structures in the near wake of a circular cylinder in sinusoidally oscillating flow. Journal of Fluids and Structures 27, 885–902.
Spidsoe, N., Karunakaran, D., 1996. Nonlinear dynamic behaviour of jack-up platforms. Marine Structures 9, 71–100.
Williamsion, C.H.K., 1985. Sinusoidal flow relative to circular cylinders. Journal of Fluid Mechanics 155, 141–174.
Yusof, J.M., 1996. Interaction of massive particles with turbulence (Ph.D. thesis), Cornell University, USA.
Zheng, W., Dalton, C., 1999. Numerical prediction of force on rectangular cylinders in oscillating viscous flow. Journal of Fluids and Structures 13, 225–249.
Zhao, M., Cheng, L., Zhou, T., 2011. Three-dimensional numerical simulation of oscillatory flow around a circular cylinder at right and oblique attacks. Ocean Engineering 38, 2056–5069.